Available online at www.sciencedirect.com
ScienceDirect
Applied Catalysis B: Environmental 80 (2008) 98–105
APPLIED CATALYSIS B: ENVIRONMENTAL
www.elsevier.com/locate/apcatb

Effects of CeO_2 addition on Ni/Al_2O_3 catalysts for the reaction of ammonia decomposition to hydrogen

Weiqing Zheng, Jian Zhang, Qingjie Ge, Hengyong Xu *, Wenzhao Li

Natural Gas Utilization, Applied Catalysis Laboratory, Dalian Institute of Chemical Physics, Graduate School of the Chinese Academy of Sciences, 457 Zhongshan Road, Dalian 116023, China

Received 12 September 2007; received in revised form 6 November 2007; accepted 12 November 2007
Available online 19 November 2007

Abstract

Effects of CeO_2 addition on the catalytic performance of Ni/Al_2O_3 catalysts for ammonia decomposition to hydrogen were investigated by activity studies and some physico-chemical methods like N_2-adsorption/-desorption, H_2-chemisorption, X-ray diffraction (XRD), H_2 temperature-programmed reduction (H_2-TPR) and NH_3 temperature-programmed surface reduction (NH_3-TPSR). The results showed that the addition of CeO_2 greatly improved the catalytic activity and stability of Ni/Al_2O_3 catalysts for ammonia decomposition to CO_x-free hydrogen. 98.3% NH_3 conversion and 32.9 mmol/(min g_{cat}) H_2 formation rate were achieved over CeO_2 promoted Ni/Al_2O_3 catalyst at 823 K and 30 000 ml/(h g_{cat}) NH_3 space velocity. The characterization results indicate that the addition of CeO_2 enlarged the catalyst pores, moderated the interaction between Ni and alumnia, suppressed Ni^0 crystallites from sintering, and improved the recombinative desorption of N adatoms from the Ni^0 surface.

Keywords: Ni-based catalyst; CeO_2 promotion; Hydrogen production; Ammonia decomposition

1. Introduction

In order to reduce the pollution arising from automobile exhausts and small-scale power generation units, hydrogen has been extensively researched as the ultimate clean energy carrier [1]. Nowadays, the exploration of the most efficient, economical, and secure procedures and sources to produce hydrogen is still one of the hot topics in hydrogen energy fields [2]. Ammonia decomposition (AD) as means to provide CO_x-free hydrogen for fuel cell applications has attracted renewed interest due to its outstanding advantages over the conventional routes based on the carbonaceous materials [3–6]. Group VIII metals (Ru, Ni, Ir, Fe, Co and Rh) or metal carbide/nitrides (MoN_x, VC_x, MoC_x, VN_x, etc.) have been proved to catalyze the ammonia decomposition to form N_2 and H_2 [3–11]. Ru clusters on different supports (especially supported on carbon nanotubes) proved to be the most active ones [12]. However, the limited availability of noble metal makes it necessary to develop less expensive catalysts based on nonprecious metals and supports. In our previous works [9,10], high performance Ni-based catalysts for AD were successfully synthesized by co-precipitation method. 63.9% NH_3 conversion and 21.4 mmol/(min g_{cat}) H_2 formation rate could be obtained over a Ni–La/Al_2O_3 catalyst at 773 K and 30 000 ml/(h g_{cat}) ammonia space velocity. However, for the application of AD to hydrogen production, the conversion is still low. Therefore, the exploration of inexpensive and more active low temperature catalysts is still a challenge in the field of ammonia decomposition to hydrogen.

It was reported that CeO_2 addition to Ni/γ-Al_2O_3 catalysts enhanced the nickel dispersion and reactivity of carbon deposits, leading to improved catalytic activity and stability during carbon dioxide reforming of methane [13]. It also could suppress the growth of Ni crystallites and formation of inactive NiO and $NiAl_2O_4$ phases [14].

Therefore, the addition of CeO_2 into the Ni/Al_2O_3 catalyst for ammonia decomposition to hydrogen has been studied in this paper. The main objective is to improve the catalyst performance and stability by utilizing the influence of CeO_2 on the interaction of Ni and Al_2O_3.

* Corresponding author. Tel.: +86 411 84581234; fax: +86 411 84581234.
E-mail address: xuhy@dicp.ac.cn (H. Xu).

0926-3373/$ – see front matter © 2007 Elsevier B.V. All rights reserved.
doi:10.1016/j.apcatb.2007.11.008

2. Experimental

2.1. Catalyst preparation

The Ni-based catalysts were prepared by a co-precipitation method according to the procedures reported previously [9,10]. Metal nitrates [$Ni(NO_3)_2{\cdot}6H_2O$, $Al(NO_3)_3{\cdot}9H_2O$ and $(NH_4)_2Ce(NO_3)6{\cdot}6H_2O$] and ammonium carbonate [$(NH_4)_2CO_3$] with stoichiometric molar ratios were used as the starting materials. The resulting Ni–Ce/Al_2O_3 samples are designated as $N_{1.20}C_yA$, in which the symbol *y* represents the Ce/Ni atomic ratio, and the molar ratio of Ni/Al is a constant of 1.20.

2.2. Catalyst characterization

A Micromeritics ASAP 2010P automated physisorption instrument was used to measure the N_2-adsorption isotherms of the samples at liquid N_2 temperature (77 K). The specific surface area was determined from the linear portion of the BET plot. The pore-size distribution was calculated from the desorption branch of the N_2-adsorption isotherm using the Barrett–Joyner–Halenda (BJH) formula. Prior to the surface area and pore-size distribution measurements, the samples were degassed in vacuum at 623 K for 2 h to remove physically adsorbed components.

Before a H_2-chemisorption measurement, 25 mg sample was introduced into a quartz reactor, swept at 723 K in deoxygenated He for 30 min, then cooled to room temperature. After reduction at 873 K for 2 h, the sample was cooled to room temperature in deoxygenated He. The pulse adsorption was conducted at R.T. with 0.31 ml pure H_2 until saturation. The pulse adsorption of H_2 was monitored by a thermal conductivity detector (TCD).

X-ray powder diffraction (XRD) patterns of the prepared samples were measured on a Philips CM-1 (Cu Kα, l = 0.1543 nm) powder X-ray diffractometer. All calculations of particle size based on the XRD data were conducted after the deconvolution of overlapping peaks.

Temperature-programmed reductions (TPR) were carried out in a conventional setup equipped with a temperature programmable furnace. A sample of 25 mg was introduced into a tubular quartz reactor. Each sample was dried at 383 K for 30 min, calcined at 623 K for 30 min and cooled down to room temperature in Ar. TPR experiments were performed under a flow of 5% H_2/Ar (30 ml/min) from 293 to 1123 K at a constant heating rate (10 K/min). The consumption of hydrogen was monitored with a TCD.

NH_3-TPSR experiments were carried out in a commercial Micrometric Autochem 2910 apparatus. Catalysts (100 mg) were placed into a quartz U-type reactor between two quartz wool plugs. The sample was reduced in situ in 50% H_2–He using a flow of 40 ml/min and a heating rate of 5 K/min up to 873 K for 3 h and then flushed in He (40 ml/min) at the same temperature for 1 h. The pulse adsorption of NH_3 was monitored by an on-line TCD detector. After adsorption, a sweep using a He flow (40 ml/min) followed. After the gas adsorption, the temperature of the catalyst bed was raised at 5 K/min to 923 K. The TPSR process was monitored by an on-line mass spectrometer (Omnisorp. Corp.).

2.3. Reaction activity and stability

The catalytic activity measurements were carried out in a fixed-bed continuous flow quartz reactor, at atmospheric pressure. To determine the relative reactivities of all catalysts, a 100 mg sample was used in each run and the flow rate of pure NH_3 as the reactant was 50 ml/min. The reaction temperature was controlled by a programmable temperature controller and detected by a movable thermocouple inside the catalyst bed. Before the catalytic test, the catalyst was pretreated with a 50% H_2/He flow (100 ml/min) at 873 K for 4 h. A gas chromatograph (Shimadzu, 8A), equipped with a Porapak-N column and a thermal conductivity detector, was used to analyze the products.

The stability measurement was carried out in the same apparatus as above. 10 mg catalysts diluted by quartz were used in the test. The reactant mixtures consisted of 15% anhydrous NH_3 and 85% He with a total space velocity of 3 000 000 ml/(h g_{cat}). The reaction temperature was controlled at 773 K.

3. Results and discussion

3.1. The performance of catalysts

3.1.1. Catalytic test

The catalytic performances of the Ni/Al_2O_3 and Ni–Ce/Al_2O_3 catalysts, tested as function of temperature, are presented in Fig. 1. After a similar pretreatment of the catalysts, all the catalytic runs were performed over 100 mg samples with an NH_3 space velocity of 30 000 ml/(h g_{cat}). As illustrated in Fig. 1, the activity in terms of NH_3 conversion increased with increasing reaction temperature, in agreement with the endothermic

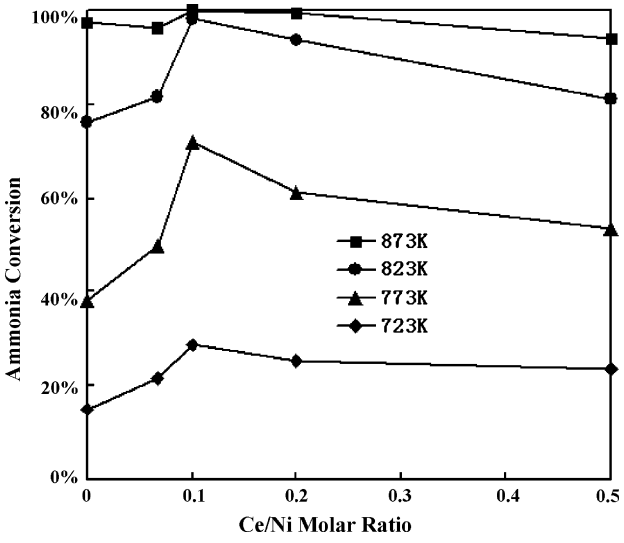

Fig. 1. Catalytic performances of $N_{1.20}A$ and $N_{1.20}C_yA$ catalysts for NH_3 decomposition at different reaction temperatures. Reaction conditions: 100 mg catalysts, 100 kPa NH_3, 30 000 ml/(h g_{cat}) NH_3 space velocity. The data are averaged within initial Time-On-Stream of 2 h.

character of the NH_3 decomposition reaction (For comparison, the equilibrium conversion increases from 99.59% and 99.90% between 723 and 873 K indicating that NH_3 decomposition is kinetically limited in this temperature window). The NH_3 conversion progressively increased with the increasing ratio of Ce/Ni up to 0.10, then decreased with further increasing ratio of Ce/Ni. These results indicate that addition of a suitable amount of CeO_2 to Ni/Al_2O_3 catalyst could evidently improve the catalytic activities of Ni/Al_2O_3. The NH_3 conversion increased from 76.3% to 98.3% at 823 K.

Table 1 gives a comparison with literature data in terms of NH_3 conversion and H_2 formation rate at 773 K. Obviously, Ni–Ce/Al_2O_3 ($N_{1.20}C_{0.10}A$ in this study) possesses the best catalytic performance for AD to hydrogen among the Ni-based catalysts, being even comparable with some Ru-based catalysts.

Stability tests were also carried out with 10 mg catalyst at, 773 K (800 K for $N_{1.20}A$), total space velocity 3 000 000 ml/(h g_{cat}) and 15 kPa NH_3, which is quite far away from the thermodynamic equilibrium conversion. Results are shown in Fig. 2. The Ce-free catalyst deactivated fast and still had not stabilized after 80 h. Obviously, the addition of CeO_2 enhanced the stability of the Ni/Al_2O_3 catalyst, because the reaction rates were practically stable before and after an unexpected power failure after 80 h which resulted in the conversion drop-off after 80 h. During that period the catalysts had been protected by He at 773 K for nearly 10 h. The reaction rate descended about 15%, then it remained stably until 175 h.

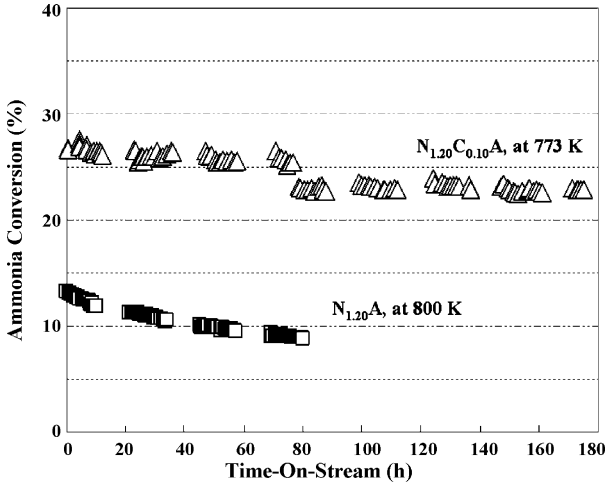

Fig. 2. Stability test of $N_{1.20}C_{0.10}A$ and $N_{1.20}A$ catalysts. Conditions: 10 mg catalysts; total space velocity 3 000 000 ml/(h g_{cat}); 15 kPa NH_3, balance He.

3.2. Characterization of catalysts

In order to investigate the reason why CeO_2 addition could increase the catalytic activity and catalytic stability of Ni/Al_2O_3 for ammonia decomposition to hydrogen, a series of characterization experiments were carried out as follows.

3.2.1. Textural property

The effects of CeO_2 addition on the textural characteristics of co-precipitated Ni/Al_2O_3 samples were studied by N_2-adsorption/-desorption and H_2-chemisorption techniques. Fig. 3 shows the N_2-physisorption isotherms of the Ce-promoted catalysts. All

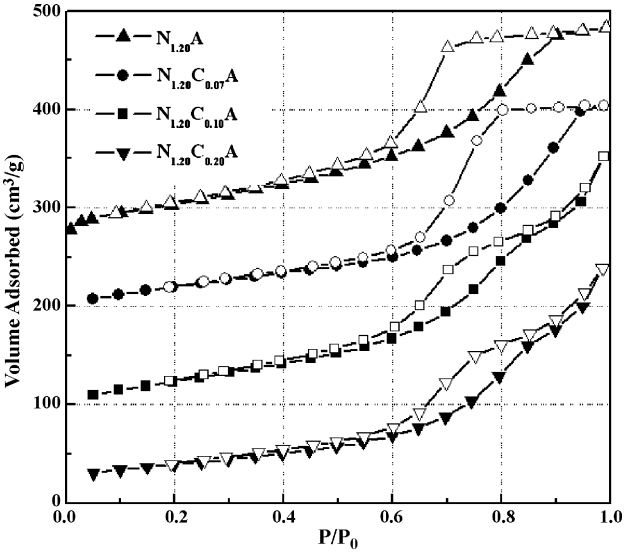

Fig. 3. N_2-physisorption isotherms of Ce promoted Ni/Al_2O_3 catalysts.

Table 1
Comparison with literature data in terms of H_2 formation and NH_3 conversion[a]

Catalysts	WHSV (NH_3)[b] ml/(h g_{cat})	Conv. *X*%	H_2 formation mmol/(min g_{cat})	TOS[c] (h)	Reference
10 wt%Ru/SiO_2	30 000	–	20.0	–	[3]
5 wt%Ru/CNT	30 000	–	28.35	3	[12]
10 wt%Ni/SiO_2	30 000	–	3.3	–	[3]
65 wt%Ni/SiO_2/Al_2O_3	30 000	–	6.8	–	[3]
5 wt%Ni/CNT	30 000	–	2.90	3	[12]
11%Ni-5%Mo/Al_2O_3	3600	78.9	–	–	[11]
4.7%Ni/MgO (Commercial)	1800	69.9	–	–	[11]
$N_{1.20}A$	30 000	38.2	12.8	2	[9]
$N_{1.20}L_{0.22}A$	30 000	63.9	21.4	2	[9]
$N_{1.20}C_{0.10}A$	30 000	71.9	24.1	2	This study

[a] AD activity test at 773 K and 100 kPa NH_3 partial pressure except for the value from Ref. [11], which was measured at 873 K.
[b] WHSV stands for weight hourly space velocity.
[c] TOS stands for initial Time-On-Stream.

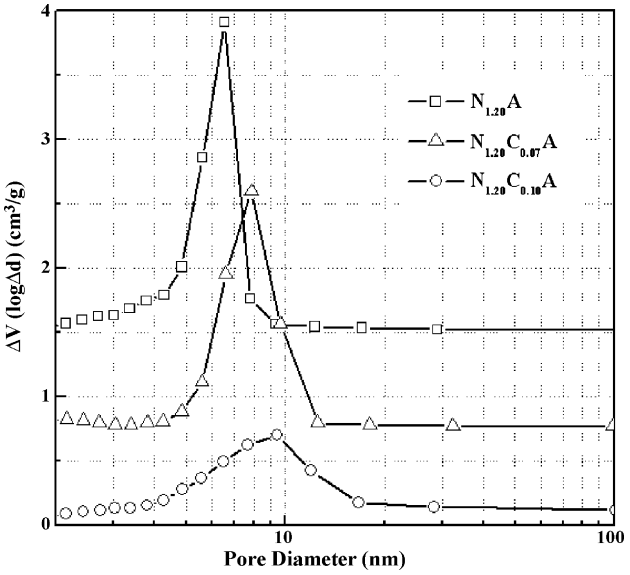

Fig. 4. Pore-size distributions Ce promoted Ni/Al_2O_3 catalysts.

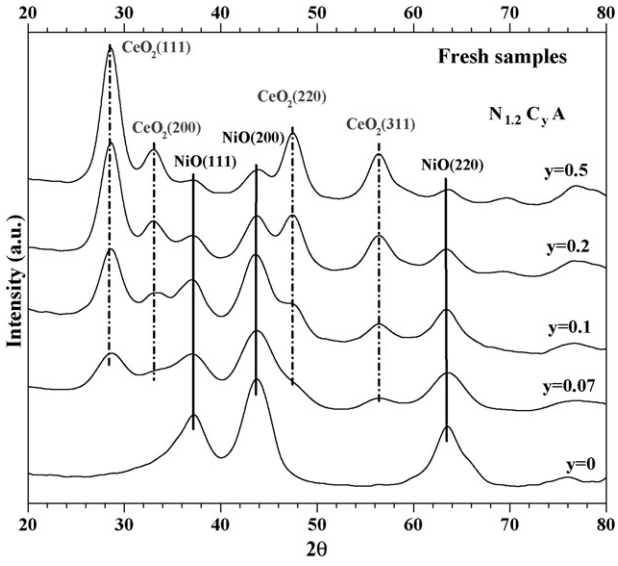

Fig. 5. Powder XRD patterns of $NiCe/Al_2O_3$ samples calcined at 873 K.

samples exhibited type IV isotherms, typical of a mesoporous texture. As a consequence of increasing Ce/Ni atomic ratios, the shape of the hysteresis loop changed from H-2 type to one resembling a quasi H-3 type, which implied that the pores structures were modified by ceria addition. As illustrated in Fig. 4 the pore-size distribution became wider.

Table 2 shows the physico-chemical properties of the catalysts. As illustrated in the table, the BET surface area of ceria promoted catalysts gradually decreased while the pore size increased, but the tendencies are not linear. With increasing ratio of Ce/Ni, both the surface areas and the pore volumes increased, passed through a maximum at Ce/Ni = 0.10, and then decreased, while the average pore size decreased from 7.9 to 6.5 nm. On the basis of our experimental results, we found that lanthanide (La or Ce) additives can enlarge the pores of the catalysts, while appropriate Ce additives tend to shrink the dimensions of the pores in the $Ni–Ce/Al_2O_3$ system which means the pores possess large volume and small average diameter.

Ni dispersion estimates, which were calculated from H_2 pulse chemisorption at 303 K using the assumption Ni:H = 1, are also listed in Table 1. Ni dispersions were increased by the addition of CeO_2 to Ni/Al_2O_3 catalysts, which indicates that the size of surface Ni particles was decreased and further promoted the reactivity. The smaller Ni particles could supply more B-5 sites which have been recognized as the active site of Ni for AD reaction [15,16]. However, with higher CeO_2 loading, a decrease in Ni dispersion is observed. An explanation could be that ceria species block the Ni particles, and further decrease the dispersion of Ni.

3.2.2. X-ray diffraction (XRD)

Figs. 5 and 6 show the XRD patterns of the calcined and reduced $N_{1.20}A$ and $N_{1.20}C_yA$ samples, respectively. Ceria, nickel and nickel oxides could be detected on the catalysts surfaces, though the patterns indicated a poor crystallinity for all samples. As expected, the characteristic peaks of NiO became gradually less intense while the CeO_2 content was increased, suggesting that the amount of detectable crystalline NiO was reduced. On the other hand, it suggested that Ni dispersion was enhanced by ceria addition (corresponding with the results of H_2-chemisorption).

CeO_2 and Ni^0 crystallite diameters of different catalysts were calculated from the line width of the CeO_2 (1 1 1) and Ni^0 (1 1 1) diffraction lines (obtained in Fig. 6) using the Scherrer equation, respectively. The results were summarized in Fig. 7 and related with catalytic performances at 773 K and 30 000 ml/(h g_{cat}) NH_3 space velocity. It can be seen that the

Table 2
Textural properties of Ni/Al_2O_3 and $NiCe/Al_2O_3$ samples

Catalysts	Ce/Ni molar ratio	BET (m^2/g)	V_P[a] (cm^3/g)	D_P[b] (nm)	Ni dispersion[c] (D_{Ni})
$N_{1.20}A$	–	216	0.383	6.8	0.13
$N_{1.20}C_{0.07}A$	0.07	171	0.356	7.9	0.14
$N_{1.20}C_{0.10}A$	0.10	181	0.426	6.5	0.21
$N_{1.20}C_{0.20}A$	0.20	139	0.367	6.5	0.22
$N_{1.20}C_{0.50}A$	0.50	147	0.299	7.6	0.15

[a] Pore volume calculated from the desorption branch of the N_2 physisorption isotherm.
[b] BJH desorption average pore diameter.
[c] H_2 pulse chemisorption.

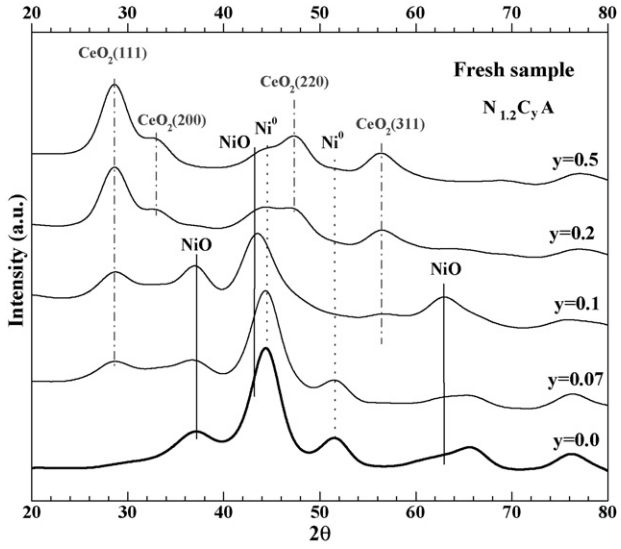

Fig. 6. Powder XRD patterns of $NiCe/Al_2O_3$ samples reduced at 873 K for 2 h (The catalysts were reduced and then removed to the analysis cell of the XRD under the protection of ultra-pure nitrogen.).

crystallite diameters of Ni^0 (1 1 1) decreased, while CeO_2 (1 1 1) ones increased with the increasing molar ratios of Ce/Ni. The results indicated that appropriate loading of CeO_2 could suppress the growth of Ni^0 on the surface, which could explain why the addition of CeO_2 enhanced the catalytic performance. In addition, the fact that CeO_2 additives improved the Ni dispersion was confirmed by H_2-chemisorption. Though the particle size of Ni^0 became smaller, the Ni dispersion decreased at higher CeO_2 loading due to the blockage of Ni particles by excessive ceria and the catalytic performance decreased as consequence.

The differences of crystallite diameters between CeO_2 and Ni^0 were quite clear except for the point of Ce/Ni = 0.10, which implies the existence of a size effect between the promoter and catalytic component. Considering the amorphous nature of the

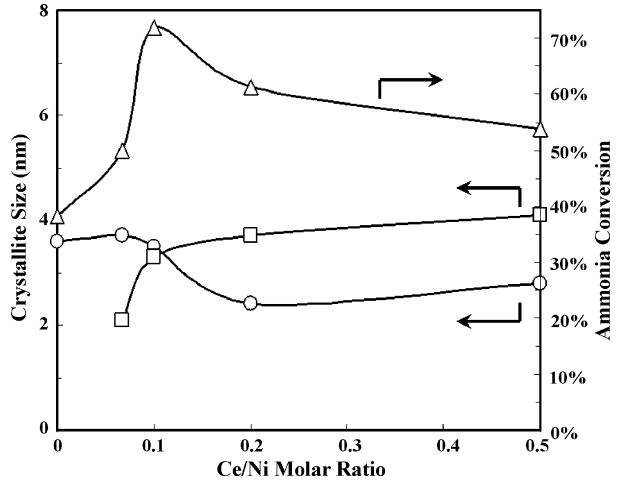

Fig. 7. Catalytic performances and crystallite diameters of CeO_2 and Ni^0 with different Ce/Ni ratios (circle: Ni^0 (1 1 1); square: CeO_2 (1 1 1); triangle: NH_3 conversion.). Conditions: Pure NH_3, 100 mg catalyst, GHSV = 30 000 ml/(h g_{cat}), reaction temperature = 773 K.

Al_2O_3 support (prepared by co-precipitation and calcined at 873 K were mainly amorphous Al_2O_3 formed, the XRD pattern of which can be found in our previous work [9]) and the limitations of the XRD technique for calculating the particle size, it is quite risky to draw that conclusion (usually, it should be confirmed by changing the particle size of the components without disturbing the contents of them [17,18]). Still, the differences between the crystallite diameters of Ni^0 and CeO_2 could influence the catalytic performance.

3.2.3. H_2-TPR analysis

Although the facts that CeO_2 could partially change the reducibility of Ni catalysts have been reported [19], the detailed changes in the Ni–Al interaction after addition of CeO_2 should be further investigated. So the effects of ceria on the reduction properties of Ni/Al_2O_3 catalysts were studied by H_2-TPR. The results are exhibited in Fig. 8, including those of pure NiO, CeO_2, CeO_2/Al_2O_3 and NiO/CeO_2 (prepared by same method with the same molar ratios as $N_{1.20}C_{0.10}A$) shown in insert (i).

The reductions of pure CeO_2 occurred around 840 K (reduction of surface ceria) and above 1100 K (reduction of bulk ceria). When Al_2O_3 was added, two small peaks were found, which were ascribed to the surface (650 K) and subsurface (840 K) ceria. It can be confirmed that the ceria existed in the form of $Ce^{(4-x)+}O^{2-}{}_{(4-x/2)}$ ($0 < x < 1$) in Ni–Ce–Al system under the reduction conditions.

The reduction of pure NiO occurred around 600–800 K. When CeO_2 was added, a peak at 660 K with a shoulder located at about 720 K and a tiny peak at 1060 K was observed. We attribute the shoulder to the reduction of NiO bound with ceria, and the latter to the reduction of bulk CeO_2. In comparison with the TPR profiles of NiO/CeO_2, the reduction of NiO was quite difficult in the Ni/Al_2O_3 ($N_{1.20}A$) system, which means the interaction between Ni and Al_2O_3 is much stronger than that in Ni/CeO_2.

When CeO_2 was added to the Ni/Al_2O_3 catalyst, some small peaks appeared in the low temperature region (<700 K) and became more obvious with the Ce/Ni ratio increasing. A symmetrical peak in the high temperature region (>1160 K) was found in $N_{1.20}C_{0.2}A$ and $Ni_{1.20}C_{0.5}A$ at high Ce content. These peaks indicated the existences of $NiO–CeO_2$ solid solutions. The former ones were ascribed to the more reducible oxygen species absorbed to the oxygen vacancies of $NiO–CeO_2$ solid solutions, and the later ones to the reduction of Ni^{2+} in the solid solutions. When Ni^{2+} ions were incorporated into the lattice of CeO_2 to replace some Ce^{4+} ions, $NiO–CeO_2$ solid solutions were formed leading to the appearance of oxygen vacancies because of the charge imbalance and lattice distortion in CeO_2, due to the differences between the radius and oxidation states of Ni^{2+} and Ce^{4+} ions. Unfortunately, diffraction peaks of $NiO–CeO_2$ solid solutions were not found in the XRD spectra, which is likely because the crystallite sizes are too small to be detected by XRD techniques. It should be noted that the formation of $NiO–CeO_2$ solid solutions had a negative effect on the catalytic performance because of the decrease of reducible NiO species due to the difficulty to reduce Ni^{2+} in solid solutions [20].

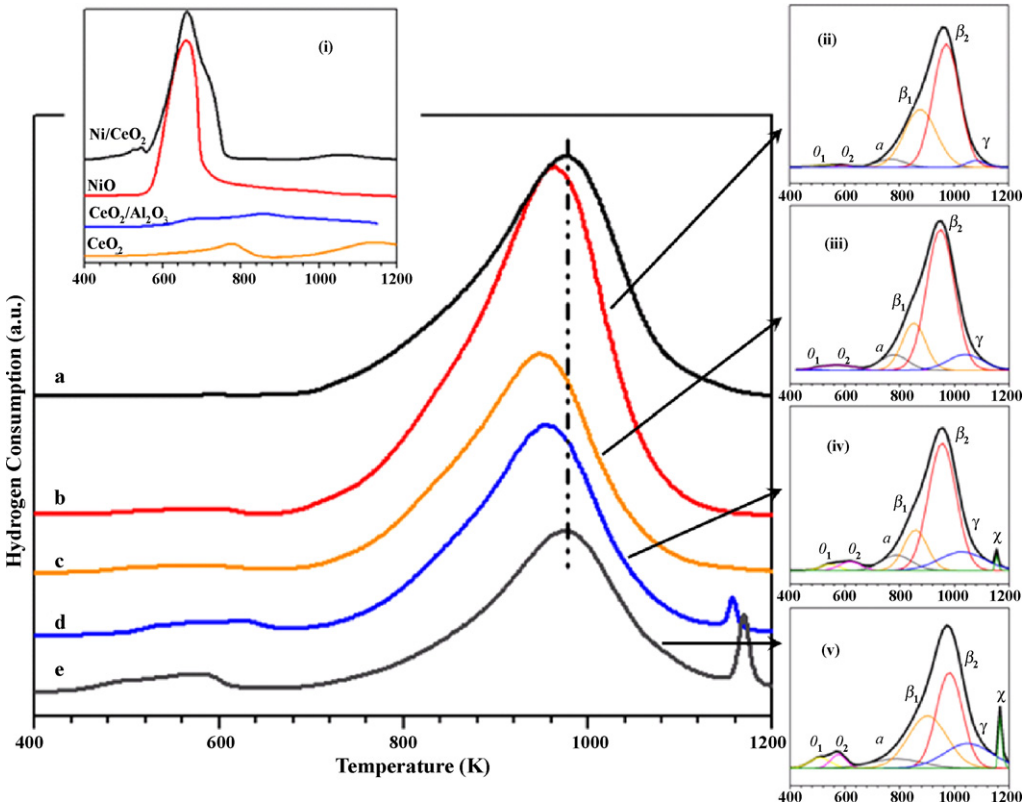

Fig. 8. TPR profiles of $N_{1.20}C_yA$ samples in 5% H_2/Ar under a heating rate of 10 K/min. (a) $y = 0$: (b) $y = 0.07$; (c) $y = 0.10$; (d) $y = 0.20$; (e) $y = 0.50$. Inserts (i) presents TPR spectra of pure NiO, CeO_2 NiO/Al_2O_3 (Ni/Al = 1.20 molar ratio) and NiO/CeO_2 (Ce/Ni = 0.10 molar ratio) samples prepared by the same method as the NiCe/Al_2O_3 ones. Inserts (ii)–(v) present the typical process for the deconvolution of the overlapping peaks, respectively.

Our previous studies indicated that the reducible NiO species in the Ni/Al_2O_3 and Ni–La/Al_2O_3 systems could be divided into four types: α-NiO (amorphous or very finely distributed reducible surface NiO species); β-NiO (Ni–Al "mixed oxides": β_1 stands for the Ni-rich phase containing some Al^{3+} ions, while β_2 stands for the Al-rich phase containing some Ni^{2+} ions); γ-NiO (nickel aluminate with a spinel structure) [9]. The range and the percentage of every reducible NiO species are listed in Table 3. The results indicated that the addition of CeO_2 could not only decrease the reduction temperature of β-NiO, but also change the fractions of NiO species. That implied that the strong interactions between Ni and Al were moderated by the Ce additives, and the reducibility was improved in consequence. Natesakhawat et al. [19] found that lanthanides, located on the catalyst surface, could act as a "spacer" by inhibiting Ni crystallites to form larger particles during reduction. We believe that this effect works not only on the surface, but also in the bulk (more like a dispersant in the Ni–Al system). As illustrated in Table 3, the fractions of α-NiO and γ-NiO were increasing with increased molar ratio of Ce/Ni, which is owed to the fact that more "spacers" supplied by CeO_2 make the separation effect more obviously. On the other hand, these "spacers" could inhibit the mobility of Ni atoms, prevent the particles from aggregating. It is known that sintering is an important cause of deactivation of Ni-based catalysts [21]. So, the addition of CeO_2 suppressed Ni from sintering, and improved the stability of Ni/Al_2O_3 for AD to hydrogen (in Fig. 2).

Table 3
TPR data of Ni/Al_2O_3 and NiCe/Al_2O_3 samples

Catalysts	Ni[a] wt%	Temperature (K)							Fraction of total area (%)						
		θ_1	θ_2	α	β_1	β_2	γ	χ	θ_1[b]	θ_2[b]	α	β_1	β_2	γ	χ
$N_{1.2}A$	49.9	–	–	767	893	984	–	–	–	–	0.4	17.7	81.9	–	–
$N_{1.2}C_{0.07}A$	49.7	537	594	769	877	972	1082	–	0.8	0.4	4.0	34.1	59.8	2.2	–
$N_{1.2}C_{0.10}A$	43.4	502	570	780	852	949	1040	–	0.1	2.9	7.0	18.4	65.5	9.1	–
$N_{1.2}C_{0.20}A$	38.2	545	618	789	858	955	1027	1157	1.7	3.0	7.9	16.3	60.5	14.4	0.8
$N_{1.2}C_{0.50}A$	28.9	509	577	788	902	982	1049	1169	3.2	3.0	7.2	31.9	39.5	18.4	2.9

[a] Obtained by XRF measurements.
[b] θ (%) = θ areas/total areas × 100%.

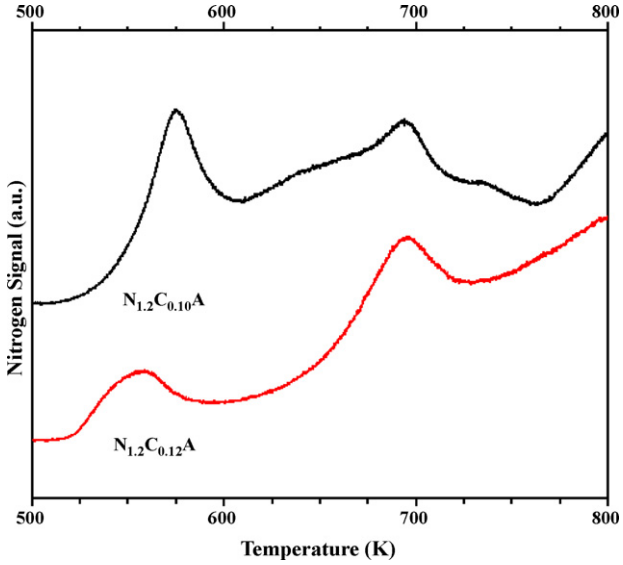

Fig. 9. N_2 formation profiles obtained from NH_3-TPSR spectra at a heating rate of 10 K/min.

3.2.4. NH_3-TPSR

Temperature-programmed surface reaction analysis can give some important information about adsorption, reaction and desorption of the reactants and products at the catalysts surface. The recombinative desorption of nitrogen adatoms is one of the slow kinetic steps of ammonia decomposition. The nitrogen atoms are the most abundant reaction intermediate [6]. Our previous kinetics results confirmed this assumption [15]. So it is important to study desorption of N atoms from the surface of Ni^0. Fig. 9 shows the spectra of N_2 signals from NH_3-TPSR.

The N recombinative desorption from Ni/Al_2O_3 catalysts was studied by NH_3-TPSR previously [15]. Results indicated that the onset of the desorption of N_2 occurred around 550 K with a single maximum between 650 and 670 K for Ni/Al_2O_3 and $Ni–La/Al_2O_3$ catalysts. In Fig. 9, it can be seen that desorption of N_2 from $Ni–Ce/Al_2O_3$ occurred mainly in two regions: <600 K and around 700 K (the baselines were increasing in the high temperature region due to a defect of the equipment) with a first maximum between 550 and 570 K and a second maximum around 690 K. It indicated that the ceria addition makes the recombinative desorption of nitrogen adatoms more facile.

There could be several reasons why N_2 desorption was facilitated after addition of ceria. The most straightforward explanation consists in the possibility that the CeO_2 promoter could enhance the proportion of highly active Ni^0 surface binding and recombination sites for N adatoms due to the better Ni dispersion (as revealed in H_2-chemisorption, TPR and XRD results). Secondly, the electronic character of Ni surface sites could be changed due to interaction with ceria. There should be some mobile electrons because ceria reacts with Ni: $Ce^{4+}(O^{2-})_{2-x}(e^-)_{2x} + Ni = Ce^{4+}(O^{2-})_{2-x}(\diamond)_{2x} + Ni(e^-)_{2x}$, ($\diamond$ represents the oxygen anion vacancy on the CeO_2 surface). As a result of the electron donation effect of ceria, the bonding of N adatoms to the Ni surface should be weakened the recombinative desorption of N adatoms could become faster [22]. It should be also noted that the well-known hydrogen spillover effect from the surface of metallic Ni [23] to ceria could mitigate the H_2 inhibition effect [4] in NH_3 decomposition that arises from the strong occupancy of active sites by adsorbed hydrogen. We cannot decide now which of these effects has the strongest influence on the recombinative desorption of N adatoms. All of them play a role probably and further studies are under way in our laboratory.

4. Conclusion

The presence of CeO_2 was found to significantly enhance the catalytic activity and catalytic stability of co-precipitated Ni/Al_2O_3 catalysts for AD to hydrogen. Over the $N_{1.20}C_{0.10}A$ catalyst 71.9% NH_3 conversion and 24.1 mmol/(min g_{cat}) H_2 formation rate could be obtained at 773 K and 30 000 ml/(h g_{cat}) NH_3 space velocity. The catalytic performance of $N_{1.20}C_{0.10}A$ catalyst is stable during 180 h continuous operation of AD to hydrogen at 773 K and 3 000 000 ml/(h g_{cat}) space velocity, which is far better than that of the Ni-based catalysts for AD. The characterization results indicate that the presence of cerium could enlarge catalysts pores, improve the dispersion of Ni, enhance the reducibility of Ni/Al_2O_3, suppress Ni^0 sintering, and facilitate the recombinative desorption of nitrogen adatoms from the surface of catalysts.

Acknowledgments

This work was supported with funds from the Ministry of Science and Technology(PRC). The authors appreciate Dr. Andreas Goldbach and Professor Yanxin Chen for helpful discussion and Dr. Yanli He for the contributions to the experiments operations.

References

[1] B.L. Yi, Fuel Cell—Principle, Technology and Application, Chemical Industry Press, Beijing, 2003.
[2] J.M. Ogden, Review of Small Stationary Reformers for Hydrogen Production, Center for Energy and Environmental Studies, Princeton University, 1999.
[3] T.V. Choudhary, C. Sivadinarayana, D.W. Goodman, Catal. Lett. 72 (2001) 197.
[4] A.S. Chellappa, C.M. Fischer, W.J. Thomson, Appl. Catal. A: Gen. 227 (2002) 231.
[5] A.T. Rassi, Proceedings of the 2002 U.S. DOE Hydrogen Program Review, NREL/CP-610-32405 (2002).
[6] S.F. Yin, B.Q. Xu, X.P. Zhou, C.T. Au, Appl. Catal. A: Gen. 277 (2004) 1.
[7] L. Li, Z.H. Zhu, Z.F. Yan, G.Q. Lu, L. Rintoul, Appl. Catal. A: Gen. 320 (2007) 166.
[8] J. Zhang, H.Y. Xu, Q.J. Ge, W.Z. Li, Catal. Comm. 7 (2006) 148.
[9] J. Zhang, H.Y. Xu, X.L. Jin, Q.J. Ge, W.Z. Li, Appl. Catal. A: Gen. 290 (2005) 87.
[10] H.Y. Xu, J. Zhang, C.Y. Yu, W.Z. Li, CN Patent 10021025.6 (2004).
[11] C.H. Liang, W.Z. Li, Z.B. Wei, Q. Xin, C. Li, Ind. Eng. Chem. Res. 39 (2000) 3694.
[12] S.F. Yin, Q.H. Zhang, B.Q. Xu, W.X. Zhu, C.F. Ng, C.T. Au, J. Catal. 224 (2004) 384.
[13] Q. Zhuang, Y. Qin, L. Chang, Appl. Catal. 70 (1991) 1.
[14] S. Wang, G.Q. Lu, Appl. Catal. B 19 (1998) 267.
[15] J. Zhang, H.Y. Xu, W.Z. Li, Appl. Catal. A: Gen. 296 (2005) 257.

[16] V. Hardeveld, V. Montfoort, Surf. Sci. 4 (1966) 396.
[17] X. Zhang, H. Wang, B.Q. Xu, J. Phys. Chem. B 109 (2005) 9678.
[18] B.Q. Xu, J.M. Wei, Y.T. Yu, Y. Li, J.L. Li, Q.M. Zhu, J. Phys. Chem. B 107 (2003) 5203.
[19] S. Natesakhawat, R.B. Watson, X.Q. Wang, U.S. Ozkan, J. Catal. 234 (2005) 496.
[20] G. Wrobel, M.P. Sohier, A. D'Huysser, J.P. Bonnelle, Appl. Catal. A: Gen. 101 (1993) 73.
[21] J. Sehested, J. Catal. 217 (2003) 417.
[22] W. Raro'g-Pilecka, D. Szmigiel, Z. Kowalczyk, S. Jodzis, J. Zielinski, J. Catal. 218 (2003) 465.
[23] Z.X. Cheng, X.G. Zhao, J.L. Li, Q.M. Zhu, Appl. Catal. A: Gen. 205 (2001) 31.